In Vivo Near-Infrared Mediated Tumor Destruction by Photothermal Effect of Carbon Nanotubes

Hye Kyung Moon,[†,‡] Sang Ho Lee,[†,§,*] and Hee Cheul Choi[†,‡,*]

[†]Department of Chemistry and Division of Advanced Materials Science, Pohang University of Science and Technology (POSTECH), San 31, Hyoja-Dong, Nam-Gu, Pohang 790-784, Korea, [‡]Department of Chemistry, Pohang University of Science and Technology (POSTECH), San 31, Hyoja-Dong, Nam-Gu, Pohang 790-784, Korea, and [§]Department of Surgery, Kosin University College of Medicine, 34 Amnam- Dong, Seo-Gu, Busan 602-702, Korea

ABSTRACT The photothermal therapy using nanomaterials has been recently attracted as an efficient strategy for the next generation of cancer treatments. Single walled carbon nanotube (SWNT) is an upcoming potent candidate for the photothermal therapeutic agent since it generates significant amounts of heat upon excitation with near-infrared light (NIR, $\lambda = 700-1100$ nm) which is transparent to biological systems including skins. Such a photothermal effect can be employed to induce thermal cell death in a noninvasive manner. Here, we demonstrate *in vivo* obliteration of solid malignant tumors by the combined treatments of SWNTs and NIR irradiation. The photothermally treated mice displayed complete destruction of the tumors without harmful side effects or recurrence of tumors over 6 months, while the tumors treated in other control groups were continuously grown until the death of the mice. Most of the injected SWNTs were almost completely excreted from mice bodies in about 2 months through biliary or urinary pathway. These results suggest that SWNTs may potentially serve as an effective photothermal agent and pave the way to future cancer therapeutics.

KEYWORDS: carbon nanotube · photothermal therapy · cancer nanotechnology · cancer therapy · near-infrared light

Despite the remarkable progresses in cancer therapeutics including conventional surgical resection, chemotherapy, radiotherapy, and their combinations, significant impediments are still unresolved, such as severe adverse reactions[1,2] and poor effectiveness against multidrug resistant cancer cells.[3,4] Recently, photothermal therapy based on nanomaterials that can be activated by a skin-penetrating NIR irradiation has been suggested as a noninvasive, harmless, and highly efficient therapeutic technique.[5−7] Among several potential photothermally active nanomaterials, SWNTs hold a particular interest because of their extraordinary photon-to-thermal energy conversion efficiency with a high absorption cross-section of NIR light.[8] Moreover, several important functions and behaviors of SWNTs in biological system that are prerequisites for the successful utilization not only in photothermal therapy but also in general biomedical applications, have been well established through intensive researches during the past decade. For example, surface functionalization of SWNTs required to improve biocompatibility and cell penetrating capability has been widely studied, through which new diagnostic device platforms for early detection of diseases,[9,10] high quality bioimaging probes,[11,12] as well as specific targeting of cancer cells[7,13] have been successfully demonstrated. The surface-tailored SWNTs also have been utilized as an efficient delivery vehicle for small anticancer drugs,[14,15] radioactive moieties,[16,17] and nucleic acid such as DNA[18,19] and siRNA[20,21] for therapeutic purposes.

Nevertheless, as similar as the most of the previously reported therapeutic applications of SWNTs, the cancer destruction by photothermal effect of SWNTs upon NIR irradiation has been attempted mostly from *in vitro* systems.[7,22−25] Consequently, some critical issues involved with the real photothermal therapeutic applications of SWNTs have not yet been confirmed, for example, whether enough thermal energy would be generated from the injected SWNTs in a living animal upon NIR irradiation, how much of the NIR flux is required to obliterate tumor cells, and whether the injected SWNTs are accumulated or removed from the body after finishing their roles. Herein, we report highly efficient *in vivo* destructions of solid tumors in mice by photothermal effect of SWNTs and their biodistributions after photothermal treatments.

RESULTS AND DISCUSSION

An aqueous biocompatible SWNT-dispersed solution was prepared by noncovalently functionalizing Hipco SWNTs with PL-PEG$_{2000}$-NH$_2$. The incorporation of polyethyleneglycol (PEG) species was guided by

*Address correspondence to gslsh@kosinmed.or.kr, choihc@postech.edu.

Received for review July 31, 2009 and accepted October 27, 2009.

Published online October 30, 2009. 10.1021/nn900904h CCC: $40.75

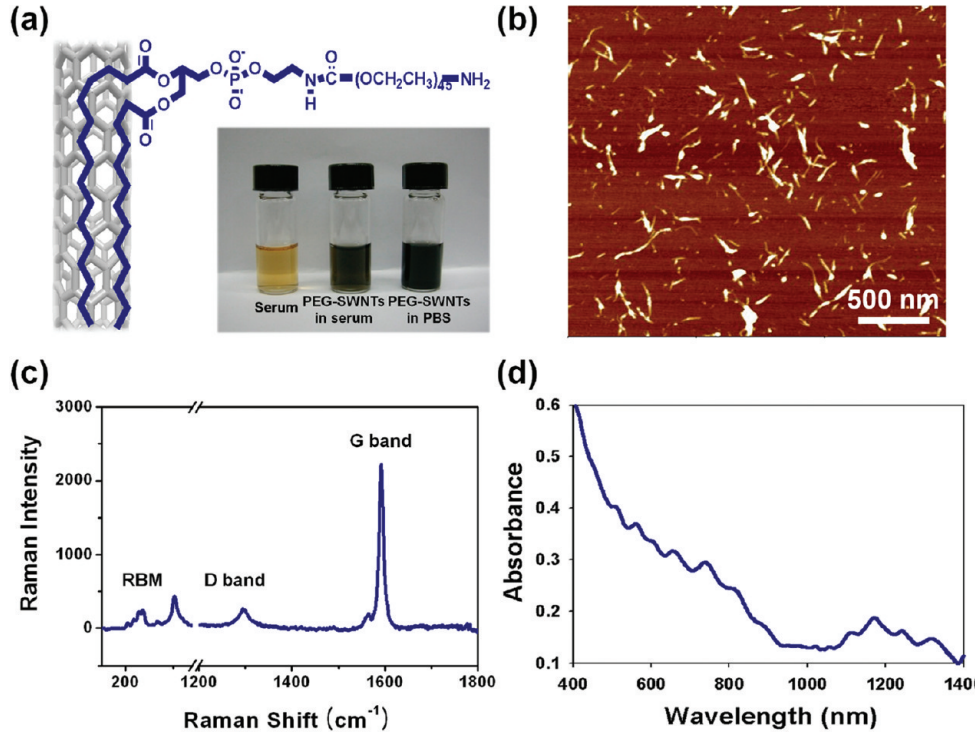

Figure 1. Aqueous solution of PEG-SWNTs. (a) Scheme of PEG-SWNTs. Strong adsorption of hydrophobic alkyl chains of phospholipid-PEG on the sidewall of SWNT. (Inset) Photographs of fetal bovine serum (FBS, left), PEG-SWNTs in fetal bovine serum (middle) and phosphate buffer salin (PBS, right). (b) Atomic force microscope (AFM) image of individual PEG-SWNTs deposited on a SiO_2. The scale bar is 500 nm. (c) Raman spectrum taken from a PEG-SWNTs solution. The G, D band and RBM are characteristic features of SWNTs. (d) UV−vis−NIR spectrum of PEG-SWNTs. The well-resolved absorption peaks indicate that the electronic energy states of individual PEG-SWNTs are well maintained after pegylation.

strong adsorption of phospholipids (PLs) to the sidewalls of SWNTs. The PEG-coated SWNTs (PEG-SWNTs) were highly dispersible in serum (fetal bovine serum) without any severe aggregation or precipitation over three weeks (Figure 1a), which agrees well with the previous result.[7] The atomic force microscopy (AFM) studies revealed that the PEG-SWNTs were well dispersed and present as either individual forms or small bundles rather than large-size aggregated bundles. The average lengths and the diameters of PEG-SWNTs were about 50−300 nm and 2−5 nm, respectively (Figure 1b). Meanwhile, intrinsic electronic and spectroscopic properties of SWNTs were not significantly affected by the adsorption of PEG molecules, as indicated by the clear preservation of four SWNT characteristic bands: radial breathing mode (RBM, 120−350 cm^{-1}), disorder related mode (D band, 1300 cm^{-1}), tangential graphite-like mode (including G^+ band, 1590 cm^{-1},[26] and G^- band, 1560 cm^{-1}) (Figure 1c), as well as by the well-resolved absorption characteristics corresponding to the electronic transitions according to the van Hove singularities from UV−vis−NIR spectroscopy (Figure 1d).[8,27]

The photothermal effect of SWNT was first examined *ex vitro* by irradiating NIR (λ = 808 nm, 3.8 W/cm^3) to the PEG-SWNTs solution. When NIR was irradiated, the temperature of the solution was increased quite rapidly. The final temperature as well as the temperature increase rate of the solution turned out to be determined by the concentration of PEG-SWNTs in solution (Figure S1a in Supporting Information). For example, even boiling phenomenon was observed upon NIR irradiation for 10 min to the solution of 140 mg/L, as water vapor droplets were instantly formed on the wall of a beaker (Figure S1b in Supporting Information). On the contrary, a negligible temperature change was monitored when phosphate buffer saline (PBS) without SWNTs was irradiated with NIR. To verify if the temperature increase was indeed originated from SWNTs rather than PEG molecules, we tested the NIR irradiation effect for a PBS solution containing PEG molecules only. As shown in Figure S1a, no significant temperature increase was observed from the PEG-containing PBS solution. These results indicate that optoelectronic excitation of SWNT by NIR irradiation occurs rapidly and the extra energies are efficiently transferred into molecular vibration modes to generate significant amounts of thermal energy.[22,27]

After confirming the photothermal effect of PEG-SWNTs, we attempted *in vivo* therapeutic examinations against nude mice bearing human epidermoid mouth carcinoma KB tumor cells (Korean Cell Line Bank) on their backs. A schematic representation about *in vivo* photothermal treatment is shown in Figure 2a. In 2 days after the KB tumor cells were xenografted on mice backs, the tumor sizes became approximately 70 mm^3 (Figure 2b). The PEG-SWNTs

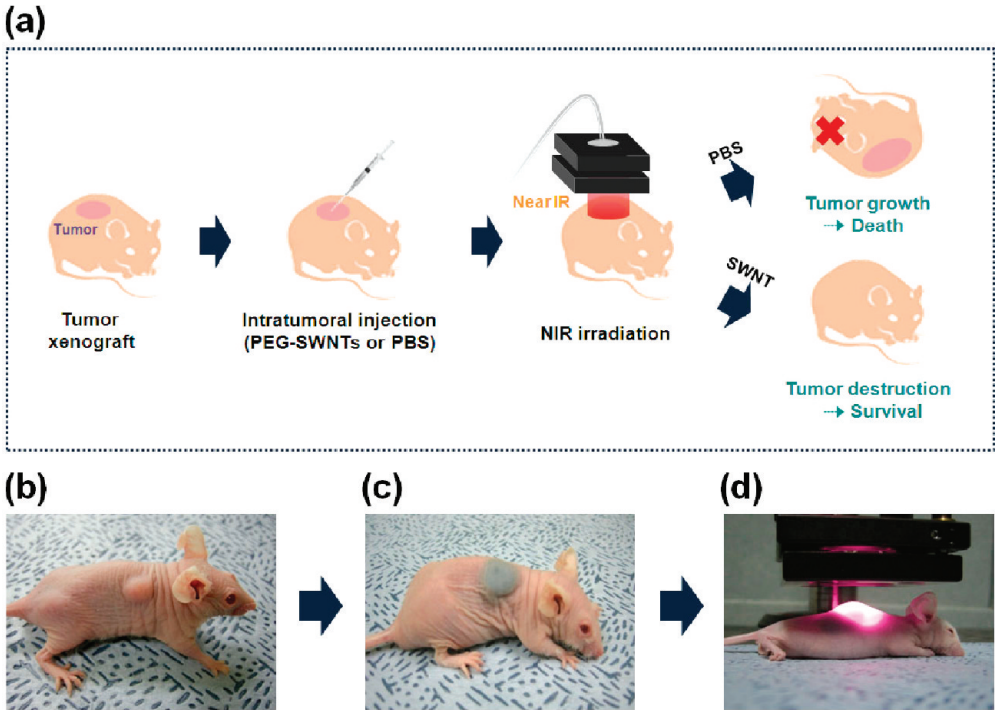

Figure 2. Photothermal treatments for *in vivo* tumor ablation using PEG-SWNTs: (a) schematic view of the procedure and results of PEG-SWNTs mediated photothermal treatment of tumors in mice; (b) photograph of a mouse bearing KB tumor cells (~70 mm^3); (c) photograph of a mouse after intratumoral injection of PEG-SWNTs solution (~120 mg/L, 100 μL); (d) photograph of near-infrared irradiation (808 nm, 76 W/cm^3) for 3 min to tumor region.

(~120 mg/L, 100 μL) were then injected into the tumor regions *via* intratumoral injection, and the color of the skin turned into dark gray due to the original color of PEG-SWNTs (Figure 2c). A mouse ready for the irradiation was located under the focal lense through which NIR could be focused to have a power density of 76 W/cm^3 and irradiated for 3 min (Figure 2d). Figure 3 shows tumor volume changes of representative mice treated in different experimental groups (one (I) for the main experiment and three (II, III, IV) for control experiments) at various post-treatment periods: (I) (PEG-SWNTs + NIR) A solution of PEG-SWNTs was injected to mice bearing KB cells, then NIR was immediately irradiated on the tumor region for 3 min; (II) (untreated) mice bearing KB cells were simply monitored without any other treatment; (III) (PBS + NIR) a PBS solution was injected followed by immediate irradiation with NIR; and (IV) (PEG-SWNTs) a solution of PEG-SWNTs was injected without NIR irradiation.

As clearly shown in Figure 3a, the mice treated with PEG-SWNTs and NIR irradiation (I) showed complete destructions of tumors after 20 days of the treatments. One noticeable observation is that there were black round marks on the mice skins when treated with (I) (Figure 3a, I, 2 Day and 14 Day). This black mark is a skin burn scar which is a direct evidence of the generation of excessive local heating from PEG-SWNTs by NIR. In contrast, there was no noticeable sign of temperature increase from the mice treated with PBS followed by NIR irradiation. Although we admit that the precise determination of therapeutic effect at the earlier stage is subtle because of the skin burn marks until 20 days after the treatments, it seems that the photothermal effect is very prompt since we frequently observe rapid disappearance of solid tumors right after the photothermal treatments. Moreover, the photothermally treated mice were quite healthy without toxic effects, abnormal behavior, or recurrence of tumors over six months (Movie S1 in Supporting Information). On the other hand, tumors treated in the control groups II through IV were continuously grown, leading to fatal status of the mice. Such four-group (I through IV) treatment experiments were repeated for another four independent sets, and the results were very reproducible as all of the mice treated with I showed dramatic destructions of solid tumors (Figure 3b). The photothermal therapeutic effect was also analyzed quantitatively by monitoring the tumor growth rates in terms of tumor volume changes as a function of time per each treatment (Figure 3c). While the tumors in the mice treated with II through IV were continuously grown up, the tumor sizes of the mice treated with I displayed almost zero volume.

Histological examinations of tumor tissues from each group further confirmed the successful destruction of tumor cells by the photothermal effect of PEG-SWNTs (Figure 4). According to the hematoxy-

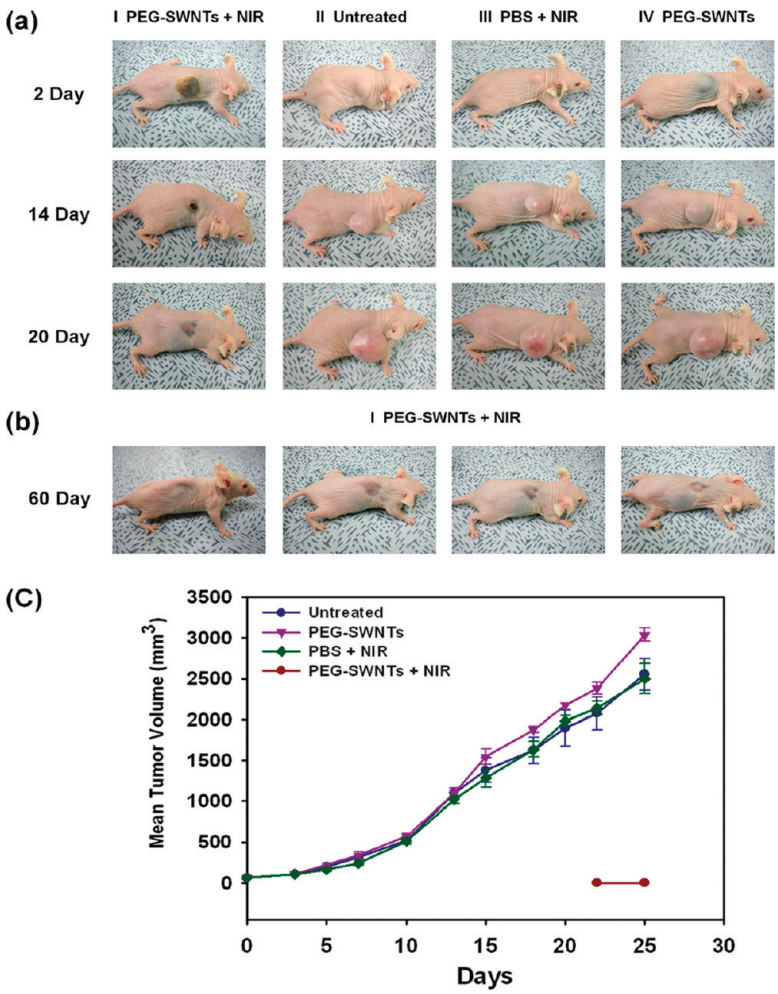

Figure 3. ***In vivo*** **photothermal effects of PEG-SWNTs for tumor obliteration. (a) Representative photographs of the mice treated in different groups at various time points after each treatment (I, PEG-SWNTs + NIR; II, untreated; III, PBS + NIR; IV, PEG-SWNTs). (b) Four mice after 60 days of photothermal treatments (I) from four independent sets. (c) Time-dependent tumor growth curves of KB tumor cell xenografts. Tumor volumes were measured three times a week after sample treatments. The results are presented as the arithmetic means with standard deviations of tumor volumes in each group (*n* = 4). Only the PEG-SWNTs + NIR treated group (I) shows significant suppression of tumor growth compared with other experimental groups (*n* = 4, $p < 0.05$, two-way ANOVA).**

lin and eosin (H & E) staining results, common features of thermonecrosis such as loss of nucleus, cell shrinkages, and coagulation were found from the tumor tissues treated with PEG-SWNTs + NIR (Figure 4a). Extensive thermonecrotic or apoptotic cells could be also evidently identified by TUNEL assay, in which dead cells are stained in brown. As shown in Figure 4d, only the tumor cells treated with PEG-SWNTs and NIR exhibited brown color within the cells, while robust and viable tumor cells were remaining with no obvious thermal damage from both untreated and PBS + NIR treated groups (Figure 4b,c, e,f). To check the presence/absence of residual tumor cells in the photothermally treated region, histological examinations were repeated again at 25 days after the complete recovery from skin damage. By analyzing histologic specimen thoroughly, we could confirm that most of the tumors were removed from the photothermally treated region as it displayed similar feature to normal skin tissue (Figure S2 in Supporting Information).

One of the important concerns after accomplishing photothermal therapy is whether the PEG-SWNTs are accumulated in tissues/organs or cleared out of the body. By utilizing the intrinsic and sensitive Raman scattering properties of SWNTs, the amounts of SWNTs accumulated in various tissues/organs were measured without additional radio- or fluorescent labeling.[26] For quantitative measurements of SWNT concentrations, standard solutions containing PEG-SWNTs at various concentrations were first examined with Raman spectroscopy to establish a calibration curve. As shown in Figure S3 (Supporting Information), strong G bands were exhibited at around 1590 cm^{-1}, of which intensities were directly proportional to the concentrations of PEG-SWNTs. The tissue/organ lysates samples were prepared by sacrificing mice at 1, 3, 7, 20, 40 days after intratumoral injection of PEG-SWNTs (~120 mg/L, 100 μL) and NIR irradiation (76 W/cm^3, 3 min). The relative amounts of SWNT in the various tissues/organs are represented as %ID/g (percentage of injected dose per gram) in Figure 5a. After 1 day of the treatments, significant amounts of SWNTs were detected from, in order, muscle where PEG-SWNTs were originally injected, spleen, blood, and skin, while little was observed from other organs including kidney. Until 7 days of the treatments, the levels of SWNTs in blood and liver were gradually increased but the level of SWNTs in muscle was remarkably decreased. The spleen showed a similar level of %ID/g at this period. However, after 7 days of the treatments, the levels of SWNTs from all of the organs were rapidly decreased, and ultimately the overall levels of %ID/g were dropped to nearly zero over time.

These findings suggest that the injected SWNTs primarily remain in muscle and skin, but they are slightly diffused into blood as the time spans over. At early stage, the diffused PEG-SWNTs were circulated in blood then prominently accumulated in spleen and liver which are related with reticuloendothelial system (RES). Such a RES uptake is known to be a general phenomenon on the fate of SWNTs with and without functionalization, primarily due to the role of mononuclear phagocytes.[16,26,28−30] Since the levels of SWNTs in RES organs were clearly decreased as a function of time, we assumed that the majority of PEG-SWNTs would be excreted from the body. According to the report by Liu *et al.*,[26] there are two possible excretion pathways of PEG-SWNTs: PEG-SWNTs bigger than 100 nm in lengths

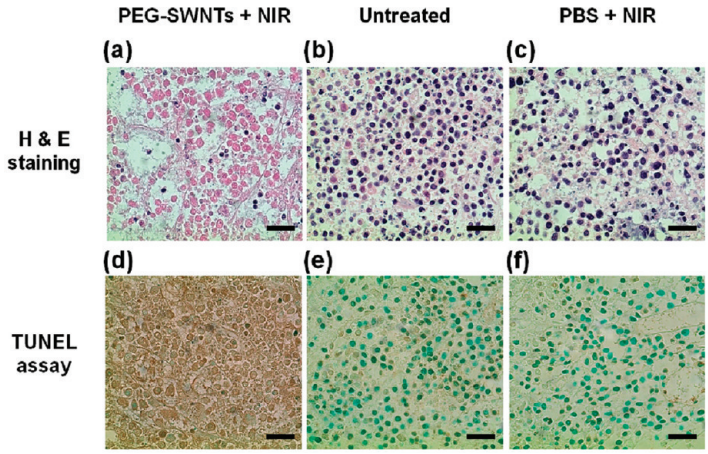

Figure 4. Histologic assessments of tumor tissues after photothermal treatments. (a−c) Hematoxylin and eosin staining (H & E) of tumor tissue from (a) PEG-SWNTs + NIR group, (b) untreated group, (c) PBS + NIR group. Most pink-stained cells represent apoptotic or necrotic cells (pink staining, cytoplasm; violet staining, nucleus). (d−f) Deoxynucleotidyl transferase biotin-dUTP nick-end labeling (TUNEL) assay for the detection of apoptotic or necrotic cells in tumor tissues from PEG-SWNTs + NIR group (d), untreated group (e), and PBS + NIR group (f). The apoptotic cells were stained brown (TUNEL positive) and non-apoptotic cells were visualized green (TUNEL negative) by counterstaining with methyl green. Data shown are representative regions. The scale bar is 50 μm.

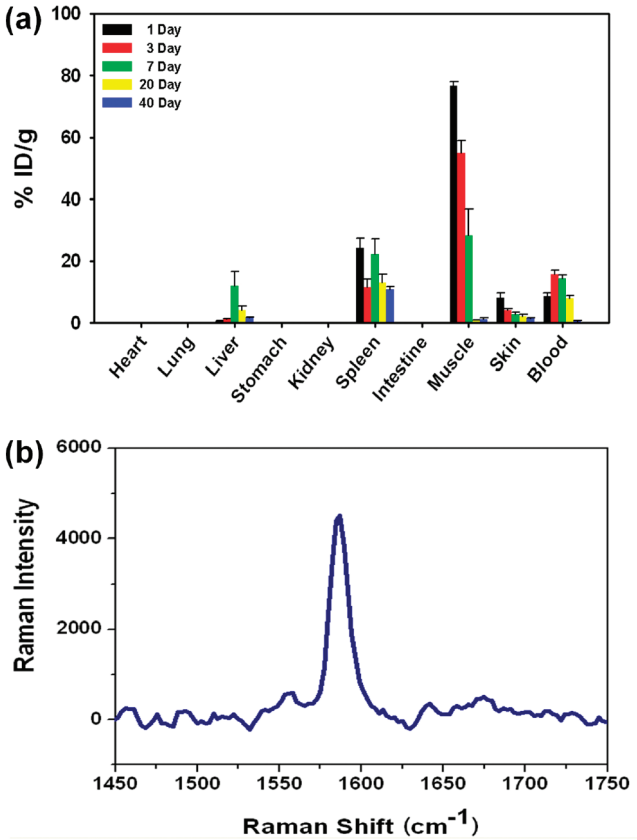

Figure 5. *In vivo* biodistribution and clearance of PEG-SWNTs. (a) Biodistribution of intratumorally injected PEG-SWNTs (~120 mg/L, 100 μL) in various tissues/organs. The data expressed as the arithmetic means ± standard error (n = 3). (b) Raman spectrum of urine dropped on a Si. The urine samples were collected for 18 days from mice treated with PEG-SWNTs and NIR. A drop of urine sample was measured using a Raman spectrometer (laser excitation wavelength of 785 nm, 317.9 mW of power, 30 s of collection time, 2 scans, ICRM7000, Lambda Ray Co., Korea).

exceeding the renal excretion are known to be easily accumulated in the liver, then excreted *via* the biliary pathway, ending up in feces. Meanwhile, very short PEG-SWNTs (<50 nm in length, diameter of 1−2 nm) are excreted through the urinary pathway. In our study of biodistribution of PEG-SWNTs, the decreased level of PEG-SWNTs in RES organs proposes that most of PEG-SWNTs were eliminated from mice bodies through biliary pathway. Furthermore, the Raman signal in collected urine over 18 days (Figure 5b) supports the excretion of short PEG-SWNTs as well. Actually, the biodistribution displays quite different patterns depending on the type of functionalization of SWNTs,[31,32] suggesting that various types of functionalization have a significant effect on the *in vivo* behaviors of SWNTs. Nevertheless, our results about the biodistribution and clearance of PEG-SWNTs agree well with previous reports.[16,26,28]

CONCLUSION

We demonstrated the photothermal effect of PEG-SWNTs upon NIR irradiation to destruct solid malignant tumors *in vivo*. When NIR was irradiated on the tumor region into which PEG-SWNTs were intratumorally injected in advance, high thermal energy was generated from the optically excited PEG-SWNTs enough to destroy tumor cells in a noninvasive manner. Although partial skin damages occurred, the SWNT-based photothermal treatment showed complete eradications of solid malignant tumors without toxicity or abnormal behavior or recurrence of tumors for a long period of time. Moreover, the issue concerned with residual SWNTs in the body after the treatment was resolved as most of SWNTs were excreted through biliary or urinary pathway by monitoring their biodistributions in various tissues/organs.

These preliminary results successfully proved that SWNT-mediated photothermal therapy is a highly feasible cancer therapeutic approach. Nevertheless, several important challenges still remain for effective and practical therapeutic usages. The most important issue, as we currently are investigating, is the selective destruction of cancer cells with minimal toxic effects on normal cells. This concern will be resolved when the photothermal treat-

ments are performed using SWNTs specifically functionalized with tumor targeting moieties such as specific ligand[7,12] or antibodies.[13,33] Having efficient photothermal capabilities with excellent specificity toward cancer cells, SWNTs can be a powerful therapeutic agent for future cancer treatments.

MATERIALS AND METHODS

Preparation and Characterization of PEG- SWNTs Solution. A solution of PEG-SWNTs was prepared by adding Hipco SWNTs (Carbon Nanotechnologies, Inc., USA) into an aqueous solution of 2 mg/L PL-PEG_{2000}-NH_2 (2-distearoyl-*sn*-glycero-3-phosphoethanolamine-*N*-[amino(PEG)2000]) (Avanti Polar Lipids). The mixture was then sonicated for 1 h to make a stable PEG-SWNTs dispersed solution (250 mg/L). The solution was centrifuged at 13000 rpm for 3−4 h to remove bundles and aggregates, and then the supernatant was filtrated through a polycarbonate filter (Whatman, pore size = 100 nm). The filtrates were resuspended in a 1 mL phosphate buffer solution (PBS). This filtration/resuspension cycle was repeated two more times in prior to obtain the final PEG-SWNTs solution.[26] Throughout the preparation processes, the optical absorbance of PEG-SWNTs solution was measured using a UV−vis−NIR spectrometer (UV-3600 spectrometer, Shimadzu) to determine the concentration. The morphological and spectroscopic characterizations were performed by atomic force microscopy (AFM, tapping mode, Nanoscope IIIa, Digital Instruments) and Raman spectroscopy (LabRAM ARMIS Raman microscope, Horiba Jobin Yvon), respectively. Specific conditions for Raman experiments are following: 785 nm of laser excitation wavelength, 62 mW of power, 100 μm of beam diameter, 30 s of collection time, 3 scans, macro mode.

***Ex Vitro* Experiment of Photothermal Effect of PEG-SWNTs Solution.** The PEG-SWNTs solution (140 mg/L) was serially diluted in 2 mL of PBS and irradiated using a 808 nm laser (diode laser, JENOPTIK unique-mode GmbH, Germany) on 0.9 cm of spot diameters at 3.8 W/cm^3. During the NIR irradiation, the temperature of the solution was measured with a thermocouple linked to temperature controller (Hanyoung, Korea) at every 20 s for total 3 min. Three sets per each PEG-SWNTs solution were measured.

***In Vivo* Photothermal Destruction of Tumors.** Human epidermoid mouth carcinoma, KB cell line (Korean Cell Line Bank) was cultured in RPMI 1640 medium supplemented with 10% FBS and 1% penicillin/streptomycin (all reagents from Hyclone) under 5% CO_2 atomosphere. The KB cells (1×10^7 cells) were harvested, suspended in 100 μL PBS, and subcutaneously injected into the back of male nude mice of each group ($n = 4$, 5- to 6-week-old, Balb/c). When the tumors were grown up to a volume of ~70 mm^3, the mice of each group were intratumorally injected with 100 μL of each solution (120 mg/L PEG-SWNTs solution, PBS) and immediately irradiated with continuous NIR laser to tumor region for 3 min under the ether anesthesia. The tumor size of each group was measured using a skinfold caliper, and tumor volume was calculated using the following equation: tumor volume = $ab^2/2$, where a is the maximum diameter of tumor and b is the minimum diameter of tumor.[34] All procedures for *in vivo* experiments were performed in accordance with Pohang University of Science and Technology guidelines on animal care and use.

***Ex Vivo* Histological Assessment of Tumor Tissue.** Two mice of each group were euthanized after 24 h of all treatments, and tumor tissues were resected and fixed overnight in 4% paraformaldehyde solution. Then, tumor tissues were embedded in paraffin after tissue processing. Paraffin sections of 4 μm thickness were mounted on a glass slide for histologic examinations with hematoxylin and eosin staining (H & E staining), and with terminal deoxynucleotidyl transferase biotin-dUTP nick-end labeling (TUNEL assay) to detect apoptotic or necrotic cells following standard protocol provided by Promega (DeadEnd. Colorimetric TUNEL System, Promega Corp., USA).

Raman Measurement of PEG-SWNTs for Calibration Curve. Sequentially diluted PEG-SWNTs solutions were transferred to a quartz cuvette (optical path length: 1 cm) and measured uisng a Raman spectrometer. The carbon nanotube characteristic G band[26] was observed at around 1590 cm^{-1}. The standard calibration curve against the concentration of PEG-SWNTs was plotted using Sigmaplot (version 10.0, Systat Software Inc., USA).

Raman Measurement of PEG-SWNTs in Mouse Tissues/Organs for Biodistribution. The nude mice intratumorally injected with PEG-SWNTs (~120 mg/L, 100 μL) and irradiated with NIR were sacrificed after 1, 3, 7, 20, 40 days of post-treatments. In total, 15 mice were used, 3 per each time point. For biodistribution analyses, each tissues/organs were collected, weighed, and homogenized in 3 mL of lysis buffer (1% SDS, 1% triton X, 10 mM DTT, 40 mM tris-acetate-EDTA buffer) by sonication (Vibra-Cell VCX 750 Sonicator, Sonics & Materials Inc., USA). The muscle and skin tissue samples were collected by taking both areas mainly covering the SWNTs injection spots as well as their nearby areas. Blood was also collected by pipet-suction from dissected mice bodies. Then, the G band intensity in each tissue/organ lysates was measured using a Raman spectrometer. Note that G band from SWNTs was not affected by the solvent types. The concentration of each tissue/organ lysates was calculated from a standard calibration curve and converted into a unit of %ID/g (percent injected dose per gram tissue) based on the following equation:[26]

$$\%\mathrm{ID/g} = \frac{[\mathrm{SWNT}]_{\text{tissue lysate}} \times V_{\text{tissue lysate}}}{[\mathrm{SWNT}]_{\text{injected}} \times V_{\text{injectedSWNT}} \times \text{tissue weight}} \times 100$$

Statistical Analyses. Four mice per each group were used for comparison using an analysis of variance (GraphPad Instat, GraphPad software Inc., USA). Differences between experimental groups were considered to be statistically significant at $p < 0.05$. All values were expressed as arithmetic means ± s.d. (standard deviation).

Acknowledgment. This work was supported by the National Research Foundation of Korea (NRF) grant funded by MEST (2008-04306, 2007-8-1158, 2005-01325), KOSEF through EPB center (R11-2008-052-02000). Korean Research Foundation (MOEHRD, KRF-2005-005-J13103). H.C.C. thanks the World Class University (WCU) program (R31-2008-000-10059-0).

Supporting Information Available: Figure S1−S3 and Supporting Movie S1. This material is available free of charge *via* the Internet at http://pubs.acs.org.

REFERENCES AND NOTES

1. Coates, A.; Abraham, S.; Kaye, S. B.; Sowerbutts, T.; Frewin, C.; Fox, R. M.; Tattersall, H. On the Receiving End—Patient Perception of the Side-Effects of Cancer Chemotherapy. *Eur. J. Cancer Clin. Oncol.* **1983**, *19*, 203–208.
2. Zachariah, B.; Balducci, L.; Venkattaramanabalaji, G. V.; Casey, L.; Greenberg, H. M.; DelRegato, J. A. Radiotherapy for Cancer Patients Aged 80 and Older: A Study of Effectiveness and Side Effects. *Int. J. Radiat. Oncol. Biol. Phys.* **1997**, *39*, 1125–1129.
3. Michael, M. G.; Tito, F.; Susan, E. B. Multidrug Resistance in Cancer: Role of ATP-Dependent Transporters. *Nat. Rev. Cancer* **2002**, *2*, 48–58.
4. Szakács, G.; Paterson, J. K.; Ludwig, J. A.; Booth-Genthe, C.; Gottesman, M. M. Targeting Multidrug Resistance in Cancer. *Nat. Rev. Drug Discovery* **2006**, *5*, 219–34.
5. Huang, X.; El-Sayed, I. H.; Qian, W.; El-Sayed, M. A. Cancer Cell Imaging and Photothermal Therapy in the Near-Infrared Region by Using Gold Nanorods. *J. Am. Chem. Soc.* **2006**, *128*, 2115–2120.
6. Gobin, A. M.; Lee, M. H.; Halas, N. J.; James, W. D.; Drezek, R. A.; West, J. L. Near-Infrared Resonant Nanoshells for Combined Optical Imaging and Photothermal Cancer Therapy. *Nano Lett.* **2007**, *7*, 1929–1934.

7. Kam, N. W. S.; O'Connell, M.; Wisdom, J. A.; Dai, H. Carbon Nanotubes As Multifunctional Biological Transporter and near-Infrared Agents for Selective Cancer Cell Destruction. *Proc. Natl. Acad. Sci. U.S.A.* **2005**, *102*, 11600–11605.
8. O'Connell, M. J.; Bachilo, S. M.; Huffman, C. B.; Moore, V. C.; Strano, M. S.; Haroz, E. H.; Rialon, K. L.; Boul, P. J.; Noon, W. H.; Kittrell, C.; *et al*. Band Gap Fluorescence from Individual Single-Walled Carbon Nanotubes. *Science* **2002**, *97*, 593–596.
9. Yu, X.; Munge, B.; Patel, V.; Jensen, G.; Bhirde, A.; Gong, J. D.; Kim, S. N.; Gillespie, J.; Gutkind, J. S.; Papadimitrakopoulos, F.; *et al*. Carbon Nanotube Amplification Strategies for Highly Sensitive Immunodetection of Cancer Biomarkers. *J. Am. Chem. Soc.* **2006**, *128*, 11199–11205.
10. Park, D.-W.; Kim, Y.-H.; Kim, B. S.; So, H.-M.; Won, K.; Lee, J.-O.; Kong, K.-J.; Chang, H. J. Detection of Tumor Markers Using Single-Walled Carbon Nanotube Field Effect Transistors. *Nanosci. Nanotechnol.* **2006**, *6*, 3499–3502.
11. Leeuw, T. K.; Reith, R. M.; Simonette, R. A.; Harden, M. E.; Cherukuri, P.; Tsyboulski, D. A.; Beckingham, K. M.; Weisman, R. B. Single-Walled Carbon Nanotubes in the Intact Organism: Near-IR Imaging and Biocompatibility Studies in Drosophila. *Nano Lett.* **2007**, *7*, 2650–2654.
12. Zavaleta, C.; Zerda, A.; Liu, Z.; Keren, S.; Cheng, Z.; Schipper, M.; Chen, X.; Dai, H.; Gambhir, S. S. Noninvasive Raman Spectroscopy in Living Mice for Evaluation of Tumor Targeting with Carbon Nanotubes. *Nano Lett.* **2008**, *8*, 2800–2805.
13. Ou, Z.; Wu, B.; Xing, D.; Zhou, F.; Wang, H.; Tang, Y. Functional Single-Walled Carbon Nanotubes Based on an Integrin $\alpha_v\beta_3$ Monoclonal Antibody for Highly Efficient Cancer Cell Targeting. *Nanotechnology.* **2009**, *20*, 105102–105109.
14. Liu, Z.; Sun, X.; Nakayama-Ratchford, N.; Dai, H. Supramolecular Chemistry on Water-Soluble Carbon Nanotubes for Drug Loading and Delivery. *ACS Nano* **2007**, *1*, 50–56.
15. Dhar, S.; Liu, Z.; Thomale, J.; Dai, H.; Lippard, S. J. Targeted Single-Wall Carbon Nanotube-Mediated Pt(IV) Prodrug Delivery Using Folate as a Homing Device. *J. Am. Chem. Soc.* **2008**, *130*, 11467–11476.
16. Liu, Z.; Weibo Cai, W.; He, L.; Nakayama, N.; Chen, K.; Sun, X.; Chen, X.; Dai, H. *In Vivo* Biodistribution and Highly Efficient Tumour Targeting of Carbon Nanotubes in Mice. *Nat. Nanotechnol.* **2006**, *2*, 47–52.
17. Singh, R.; Pantarotto, D.; Lacerda, L.; Pastorin, G.; Klumpp, C.; Prato, M.; Bianco, A.; Kostarelos, K. Tissue Biodistribution and Blood Clearance Rates of Intravenously Administrated Carbon Nanotube Radiotracers. *Proc. Natl. Acad. Sci. U.S.A.* **2006**, *103*, 3357–3362.
18. Singh, R.; Pantarotto, D.; McCarthy, D.; Chaloin, O.; Hoebeke, J.; Partidos, C. D.; Briand, J.-P.; Prato, M.; Bianco, A.; Kostarelos, K. Binding and Condensation of Plasmid DNA onto Functionalized Carbon Nanotubes: Toward the Construction of Nanotube-Based Gene Delivery Vectors. *J. Am. Chem. Soc.* **2005**, *127*, 4388–4396.
19. Wu, Y.; Phillips, J. A.; Liu, H.; Yang, R.; Tan, W. Carbon Nanotubes Protect DNA Strands during Cellular Delivery. *ACS Nano* **2008**, *2*, 2023–2028.
20. Zhang, Z.; Yang, X.; Zhang, Y.; Zeng, B.; Wang, S.; Zhu, T.; Roden, R. B. S.; Chen, Y.; Yang, R. Delivery of Telomerase Reverse Transcriptase Small Interfering RNA in Complex with Positively Charged Single-Walled Carbon Nanotubes Suppresses Tumor Growth. *Clin. Cancer Res.* **2006**, *12*, 4933–4939.
21. Liu, Z.; Winters, M.; Holodniy, M.; Dai, H. siRNA Delivery into Human T Cells and Primary Cells with Carbon-Nanotube Transporters. *Angew. Chem., Int. Ed.* **2007**, *46*, 2023–2027.
22. Panchapakesan, B.; Lu, S.; Sivakumar, K.; Taker, K.; Cesarone, G.; Wickstrom, E. Single-Wall Carbon Nanotube Nanobomb Agents for Killing Breast Cancer Cells. *Nanobiotechnology* **2005**, *1*, 133–139.
23. Chakravarty, P.; Sainz, R.; Li, S.; Dumortier, H.; Lacerda, L.; Kostarelos, K.; Giordani, S.; Prato, M. Thermal Ablation of Tumor Cells with Antibody-Functionalized Single-Walled Carbon Nanotubes. *Proc. Natl. Acad. Sci. U.S.A.* **2008**, *105*, 8697–8702.
24. Wang, C.-H.; Huang, Y.-J.; Chang, C.-W.; Hsu, W.-M.; Peng, C.-A. *In Vitro* Photothermal Destruction of Neuroblastoma Cells Using Carbon Nanotubes Conjugated with GD2 Monoclonal Antibody. *Nanotechnology* **2009**, *20*, 315101–315107.
25. Shao, N.; Lu, S.; Wickstrom, E.; Panchapakesan, B. Integrated Molecular Targeting of IGF1R and HER2 Surface Receptors and Destruction of Breast Cancer Cells Using Single Wall Carbon Nanotubes. *Nanotechnology.* **2007**, *18*, 315101–315110.
26. Liu, Z.; Davis, C.; Cai, W.; He, L.; Chen, X.; Dai, H. Circulation and Long-Term Fate of Functionalized, Biocompatible Single-Walled Carbon Nanotubes in Mice Probed by Raman Spectroscopy. *Proc. Natl. Acad. Sci. U.S.A.* **2008**, *105*, 1410–1415.
27. Bachilo, S. M.; Strano, M. S.; Kittrell, C.; Hauge, R. H.; Smalley, R. E.; Weisman, R. B. Structure-Assigned Optical Spectra of Single-Walled Carbon Nanotubes. *Science* **2002**, *298*, 2361–2366.
28. Yang, S. T.; Fernando, K. A.; Liu, J. H.; Wang, J.; Sun, H. F.; Liu, Y.; Chen, M.; Huang, Y.; Wang, X.; Wang, H.; et al. Covalently PEGylated Carbon Nanotubes with Stealth Character *in Vivo*. *Small* **2008**, *4*, 940–944.
29. Cherukuri, P.; Gannon, C. J.; Leeuw, T. K.; Schmidt, H. K.; Smalley, R. E.; Curley, S. A.; Weisman, R. B. Mammalian Pharmacokinetics of Carbon Nanotubes Using Intrinsic near-Infrared Fluorescence. *Proc. Natl. Acad. Sci. U.S.A.* **2006**, *103*, 18882–18886.
30. Yang, S.-T.; Guo, W.; Lin, Y.; Deng, X.-Y.; Wang, H.-F.; Sun, H.-F.; Yuan-fang Liu, Y.-F.; Wang, X.; Wang, W.; Chen, M.; et al. Biodistribution of Pristine Single-Walled Carbon Nanotubes *in Vivo*. *J. Phys. Chem. C* **2007**, *111*, 17761–17764.
31. Villa, C. H.; McDevitt, M. R.; Escorcia, F. E.; Rey, D. A.; Bergkvist, M.; Batt, C. A.; Scheinberg, D. A. Synthesis and Biodistribution of Oligonucleotide-Functionalized, Tumor-Targetable Carbon Nanotubes. *Nano Lett.* **2008**, *8*, 4221–4228.
32. Liu, Z.; Chen, K.; Davis, C.; Sherlock, S.; Cao, Q.; Chen, X.; Dai, H. Drug Delivery with Carbon Nanotubes for *in Vivo* Cancer Treatment. *Cancer Res.* **2008**, *68*, 6652–6660.
33. McDevitt, M. R.; Chattopadhyay, D.; Kappel, B. J.; Jaggi, J. S.; Schiffman, S. R.; Antczak, C.; Njardarson, J. T.; Brentjens, R.; Scheinberg, D. A. Tumor Targeting with Antibody-Functionalized, Radiolabeled Carbon Nanotubes. *J. Nucl. Med.* **2007**, *48*, 1180–1189.
34. Yao, Y. M.; Liu, Q. G.; Yang, W.; Zhang, M.; Ma, Q. Y.; Pan, C. E. Effect of Spleen on Immune Function of Rats with Liver Cancer Complicated by Cirrhosis. *Hepatobiliary Pancreatic Dis. Int.* **2003**, *2*, 242–246.